한국기계가공학회지, 제8권, 제2호, pp.10～17 (2009. 6)
Journal of the Korean Society of Manufacturing Process Engineers, Vol 8. No. 2, pp.10～17 (2009. 6)

Development of End-milling Inspection System Using 450kVp Tube Voltage

Moon-Chul Yoon*, Jin-Seok Jung**, In-Ho Hwang**
Sun-Woo Yuk**, Su-Kang Park****, Do-Hun Chin*****

450kVp Tube Voltage를 이용한 엔드밀링 검색 시스템 개발

윤문철*, 정진석**, 황인호**, 육선우**, 박수강***, 진도훈****

(Received 05 February 2009; received in revised form 21 May 2009; accepted 23 June 2009)

ABSTRACT

Transillumination system used by radiation is widely applied to industrial imaging system. In this study, the linear detector array constructed with scintillator and pin diode, and a multi-channel data acquisition system was developed for precision inspection of end-milling. The detector module consists of 16-$CdWO_4$ crystal scintillator and photodiode array. The detector and data acquisition system was applied to precision inspection of end-mill and the images of the end-mill were successfully reconstructed. The total system can analyze the Detector Quantum Efficiency(DQE) of each system. The performance of developed photodiodes equipment was compared with each other for different crystal geometry and its characteristics. Finally fine details of the end-mill phantom were constructed for industrial application. The image acquired contains several objects on a real time data transfer and the linear X-ray scanning system can be applied to many fields of a industry.

Key Words : End-milling inspection system, Data acquisition system(DAS), Signal-to-noise ratio(SNR)

1. Introduction

An X-ray system has been used for the inspection of precision end-milling and other contraband in customs applications. Some companies have developed nondestructive inspection systems using X-ray. This inspection systems use high energy and require large areas of heavy shielding, expensive installations, and high costs of operation and maintenance. However the developed 450kVp X-ray inspection system has advantages of low installation cost, easy operation, and minimal environmental impact. In this study, A prototype X-ray scanner system consists of a 450kVp X-ray generator, a linear detector array and an electric circuit. In designing a $CdWO_4$(CWO) scintillation detector, the geometry of the CWO is determined. An experiment was also conducted to determine the optical surface treatment. A PIN photodiode has been used in the solid-state detector for X-ray detection as a

* C. A. : Department of Mechanical Engineering, PuKyong National University
E-mail : mcyoon@pknu.ac.kr
** Korea Orthopedics and Rehabilitation Eng. Center
*** Korea Electric Testing Institute
**** Kyunnam College of Information and Technology

photosensor of visible light from the CWO. The photodiode should have shallow p-layer to detect the visible light with short wavelength from the CWO. To make the photodiode of shallow junction, the photodiode is designed using a device simulation tool.

The leakage current, capacitance, and spectral response of the fabricated photodiode are measured and must be compared with those of other commercial products. A data acquisition system consisting of a dual-switched integrator, a multiplexer and analog-to-digital converter is fabricated and it is used for the actual inspection test for detecting of end-mill objects in an arbitrary container. The developed inspection system is realized by practical application for evaluating the performance of the system.

2. Materials and Methods

2.1 CWO Scintillator

Due to large X-ray absorption efficiency and small after-glow, the CWO can detect high-energy X-rays with a fast scanning time in spite of its low light output. To improve the light output and achieve high signal-to-noise ratio(SNR), it is important to increase the light number which is reaching the bottom surface of a CWO geometry. Several factors such as the incident X-ray energy, the geometry, and surface condition can have an influence on the light output from the scintillator. Ordonez et al. have optimized the scintillator size to detect low-energy radiation by controlling the total number of light obtained at the center of the scintillator block. The radiation absorption and the light collection efficiency are dominantly affected by the scintillator height (z-axis) as shown in Fig. 1(a). However, the scintillator placed parallel to the X-ray incident direction is used for high-energy (E>450kVp) X-ray detection as shown in Fig. 1(b).

This placement prevents the photodiode from being irradiated directly and it results in reduced radiation damage and noise of the electric device. To determine the scintillator size, it is not practical to control the number of light collected at the middle of a scintillator. because only a few portion among the incident X-ray contributing to the light signal can arrive at the center of the scintillator.

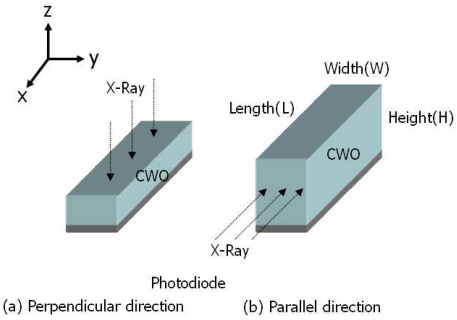

Fig.1. Geometry of detector element.

So the scintillator block CWO is divided into small subregions, each 0.2 *mm* along the direction of the X-ray penetration, and the total light output is predicted by using deposit energy and light collection efficiency in each subregion.

This size covered the mean free path of 150keV photon[1], whereas the average energy of 450kVp X-ray is about 167keV. The number of light generated in each subregion could be obtained by the product of the deposited energy and the number of light per unit energy absorbed in the subregion (15 light/kiloelectronvolts)[2-4].

Table 1 . Parameters used in Spectrum Calculation

Parameter	Value
Maximum electron energy (keV)	450
Target material	Tungsten
Target angle	20
First material and thickness	Stainless steel, 3mm
Ceramic insulator	7.5mm
Thickness of insulation oil	50mm
Diameter of X-ray vacuum tube	134mm

The absorption mean free path and scattering mean free path of the light in the CWO are both 80 *cm*[5]. The light collecting efficiency reaching the bottom surface among the light in each subregion can be obtained by DETEC97. Finally, the total light number from the overall scintillator block per incident X-ray could be calculated by summing the number of lights collected at the bottom of each subregion. The 450kVp X-ray spectrum used was predicted using MCNP4B, based on the structure of X-ray generator and the parameters in table 1.

Due to a larger X-ray absorption efficiency and lower one after glowing, $CdWO_4$(CWO) was chosen to detect lower energy X-rays. It has a fast scanning time but comparatively low light output. Therefore, it is important to increase the light collection efficiency in system by optimizing the geometry of the CWO and achieving a higher SNR. There are several factors influencing a light output, such as, X-ray energy and direction. The factors are materials, geometry and scintillator surface treatment. Energy loss of X-ray in the scintillator is a exponential function according to a penetrating depth of X-ray. The photodiodes for detecting visible light of the scintillator are coupled to the bottom its surface. Both energy deposition and light collecting efficiency must be considered to estimate the light output from a CWO reasonably.

External reflector was installed to prevent lights escaping from crystals. Three types of surface treatment in CWO were used to investigate their effects on light output. i.e., 4 ground sides/ground top, 4 polish sides/polish top and 4 polish sides/ground top. The topside surface refers to the surface of the CWO opposite the photodiode. Fig. 2, 3 and 4 show the effects of CWO geometry on light output. Fig. 2 shows the effects of crystal width on light output respectively at a height of 3.0 mm and a depth of 10.0 *mm*. As shown in Fig. 2, light output increases along with crystal width and finally saturates about 5 *mm* after. A trade-off between a spatial resolution and sensitivity should be considered to determine the optimum crystal width.

Fig. 3 shows the effects of crystal height on the light output respectiveely at a width of 1.7 *mm* and a length of 10.0 *mm*. A maximum peak appears about 3.0 *mm* in Fig. 3. Light output decreases after this peak because of the decrease of the light collection efficiency.

Fig. 4 shows the effects of crystal depth on light output according to a fixed crystal width and height of 1.7 *mm* and 3 *mm*, respectively. Also it shows that light output increases along with crystal depth and it saturates after depth of 10 *mm*. So the amount of energy absorption does not increase even if depth is increased. The CWOs with ground surfaces produce more light than those with (a) or (b) surfaces. And some studies have suggested that a polished surface is more efficient. Also the differences of light efficiency are due to the effects of surface treatment, the properties of crystal materials, crystal geometry and the location of light in a crystal. Our results indicate that in polished crystals, a considerable amount of scintillation light is trapped internally and it cannot reach the photodiode.

However, ground surfaces break up internal reflections and direct light down toward the photodiode preferentially. Therefore, ground surfaces yield more light than polished surfaces.

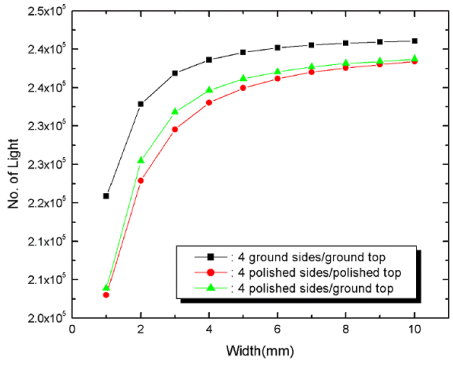

Fig. 2 Effects of crystal width on total light output in $CdWO_4$

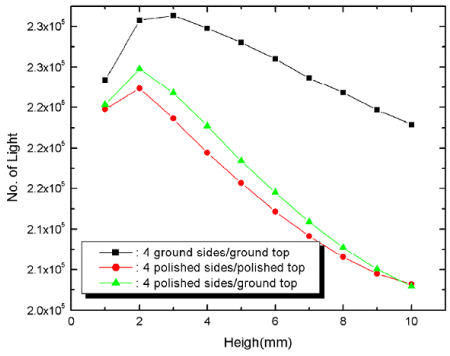

Fig. 3 Effects of crystal height on total light output in $CdWO_4$

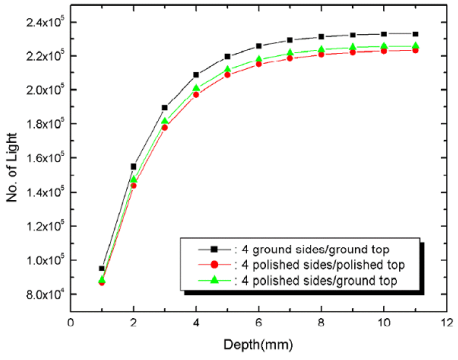

Fig. 4 Effects of crystal depth on total light output in $CdWO_4$

It shows that a CWO of 1.7 *mm*(W) × 3.0 *mm*(L) × 10.0 *mm*(D) with a surface treatment of 4 ground sides and a ground top is optimal geometry for detecting 450kVp X-ray[8].

2.2 Detector Module

16 channel linear detector module were fabricated by bonding CWO crystal block onto a silicon PIN photodiode. The detector pitch in the array is 2.0 *mm* and the gap of 0.3 *mm* was filled with Ta doped with TiO_2 to prevent X-ray and light scattering between neighboring crystals. A scintillation detector was made by combining this $CdWO_4$ array with a PIN photodiode. To construct a photodiode with p-i-n structure, an intrinsic layer was prepared using an n-type silicon wafer with high resistivity (1,200-4,000Ω·㎝). Then, successive doping by diffusion make a typical layer thickness of p+_n-_n+ structure. The photodiode has an i-layer thickness of about 77μm and p-layer thickness of about 3μm. A silicon nitride layer was finally coated onto the p-layer for passivation. The use of an n-type guard ring around the active area of photodiode should be noted. And this provides a leakage current which is generated outside the active area. After the photodiode is polished and Teflon-taped to improve signal light reflection, it prevents cross talking. The photodiode has a resistivity of 30㏁ and a measured junction capacitance of 300㎊. Fig. 6 shows the Si-photodiode detector[6] coupled to a $CdWO_4$ crystal. Some performance characteristics for the photodiode are summarized in Table 2. The detector module layout and film are shown in Fig. 5 and Fig. 6.

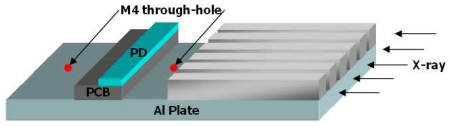

Fig. 5 X-Ray detector Module Layout

Fig. 6 16 Channel Si photodiode coupled to $CdWO_4$ crystal

Fig. 7 shows that a leakage current at a reverse 5V and a capacitance without bias are about 1nA/cm^2 and 550pF/cm^2, respectively. In Fig. 7, a sharp increase of leakage current and decrease of capacitance is shown

about reverse 5V. This sudden increase of leakage current is due to a n++-guard ring, which is doped heavily with phosphorous to reduce photodiode leakage current. The depletion layers at two different interfaces of the p+ layer / n- intrinsic layer and the n- intrinsic layer / n++guard ring may be in reverse bias and finally be combined at -5V[7]. This may cause a sharp increase in the two curves as shown in Fig. 7. Further detailed study on this abnormal increase should be identified[8-9].

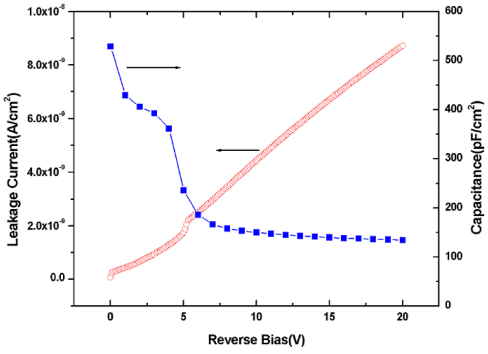

Fig. 7 Leakage current and capacitance of a PIN diode

Table 2 . Photodiode characteristics

Crystal	CdWO4
Thickness (m)	280 μm
Shunt Resistance (Ω)	30 MΩ : no bias
Junction Capacitance (F)	300 pF : no bias
Dark Current (A)	100 nA : no bias
Pixel Size (mm^2)	1mm×10mm
Photodiode Type	PIN : p+ / n-/n+
p-layer thickness (um)	3 μm
i-layer thickness (um)	77 μm

2.3 Data Acquisition System

Fig. 8 shows the DAS system and it consists of a dual-switched integrator, a programmable gain instrumentation amplifier, and a 16bit ADC. The DAS gain was set to 10^8, which was in series connection of 10^7 gain in the integrator and 10^1 gain in the instrumentation amplifier[10-11]. The ADC data are fed by the instrumentation amplifier with a sampling frequency of 500 *kHz*. For the performance test of the DAS developed, the total noise of the DAS was measured to be 200μN rms. and it could be determined by root mean square(RMS) noise of each component such as a dual integrator, PGA, MUX, and active filter. The DAS is positioned between the detector array and the computer and it performs the following three major functions: 1) amplifying the signal from detectors 2) converting the analog signal into the digital one and 3) transmitting the digital data to the computer and further image processing.

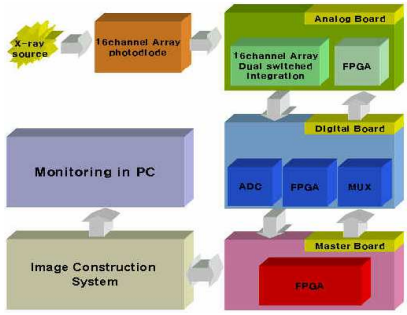

(a) DAS Block Diargram

(b) Designed DAS System

Fig. 8 Data Acquisition System

2.3.1 Analog board

The analog board is to convert from current to voltage using ACF2101. The block diagram of this analog board is shown in Fig. 9(a).

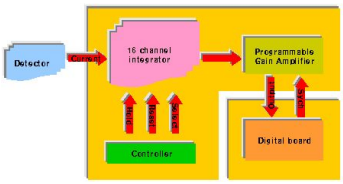

(a) block diagram

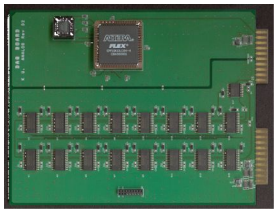

(b) Analog board

Fig. 9 Analog board

The amplifier has 120dB wide dynamic range[10] and it includes integration capacitor, reset and hold switches, and output multiplexer. The internal capacitor is using a precision of 100pF and the voltage putput, V_{out}, can be defined as

$$V_{out} = \frac{1}{-C_{INTEGRATION}} \int_{IN}^{I} dt \qquad (1)$$

2.3.2 Digital board

The digital board[12] is supposed to acquire analog signals to be sent from analog board through a multiplxer and changed to digital signals through ADC8322. The diagram of this digital board is shown in Fig. 10.

The ADS has a 16bit output and 500 *KHz* sampling rate A/D converter with an internal reference voltage of 2.5V. So maximum digit has a 65,536 due to the 16bit is 2^{16}[11].

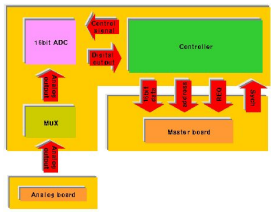

(a) block diagram

(b) A picture of the digital board

Fig. 10 Digital board

2.3.3 Master board

This board to transmit 16bit data to the PC and outputs the signal to synchronize a signal of the digital with the analog. The diagram of this master board is shown in Fig. 11(a).

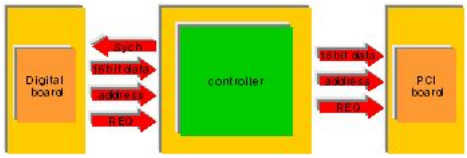

(a) block diagram

(b)A picture of the master board

Fig. 11 Master board

For the maximum SNR, the impedance between photodiode and preamplifier was accomplished by a feedback capacitor for the preamplifier. The gain,

offset compensation, bandwidth, noise, and the phase margin of the preamplifier were considered in designing. A dual-switched integrator was used to amplify the signal from a photodiode and to achieve the zero integration dead time for utilizing the detector signal fully during the scan. The signal of the analog board was amplified by 10^8. and it is delivered to the ADC through the programmable gain instrumentation amplifier as a buffered inverter. The timing signal of the ADC and the address signal of the MUX, and the control signal for the data transmission were generated in the digital logic board. This board is implemented by an field programmable gate array which was coded with hardware description language.

3. Application

According to the design method suggested in previous section, 256, 16 channel detector arrays with height of 3.0 *mm* and depth of 10.0 *mm* were fabricated to cover real container height of 4.0 *m*. A detector block size is 1.7 *mm*(W) × 10.0 *mm*(D) × 3.0 *mm*(H). The pitch in the array of detector is 2.0 *mm* and the gap of 0.3 *mm* is filled with Ta doped with TiO_2 to prevent scattering of x-rays and light between neighboring crystals. The x-ray tube used in the system produces an x-ray of 120 *Hz* with maximum energy of 450keV and average one of 167 keV. The tube voltage rises from zero to a peak of 450kV for each pulse. FWHM(Full Width at Half Maximum) and an electric current of one pulse are 30 second and 0.7A respectively. To test the performance of the detection system, the end-mill set was inspected with the developed system in this study. The end-mill table is moving with the speed of 8 *cm*/*sec* during inspection. Fig. 12 is the original photo of end-mill and is scanned using the developed system. Fig. 13 is a scanned image of end-mills and they can be distinguished from background image clearly.

Fig. 12 Each other end-milling image

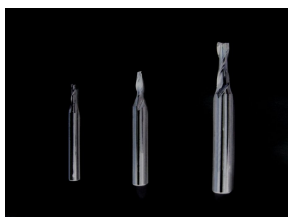

Fig. 13 End-milling inspection Image

4. Conclusion

This paper describes new design methods of X-ray detector and this total scan system used 450kVp X-ray. Design parameters decided in this paper will be used in constructing the scan system and design methods of detector can be applied to both high and low energy X-rays. In addition to the scintillator array, the PIN photodiode and DAS have also been optimized. The developed system can construct a end-milling phantom which is matching to the shape of several materials with different metal components. And this system can be applied to precision inspection system with suitable resolution that is matching to component phantom.

References

1. W. Rossner and B. C. Grabmaier, "Phosphors for X-ray detectors in computed tomography," J. Luminescience, Vol. 48/49, pp. 29-36, 1991.
2. J. G. Graeme, "Photodiode Amplifier", McGraw Hill, 1996.

3. S. W. Yuk, "A study on design of PIN photodiode coupled with pixellated scintillator for low energy detector", Ph. D Thesis of Korea Univ., 2006.
4. Y. Saitoh, T. Akamine, K. Satoh, M. Inoue, J. Yamanaka, K. Aoki, S. Miyahara, and M. Kamiya, "New profiled silicon PIN photodiode for scitillation detector", IEEE Trans, Nucl, Sci., Vol. 42, pp. 345-350, Aug. 1995.
5. T. Maisch, R. Gunzler, M. Weiser, S. Kalbitzer, W. Welser, and J. Kemmer, "Ion-implanted Si pn-junction detectors with ultra-thin windows," Nucl. Instrum, Methods, Vol. A288, pp. 19-23, 1990.
6. T. E. Hansen, "Silicon detectors for the UV- and blue spectral regions with possible use as particle detectors", Nucl. Instrum, Methods, Vol. A235, pp.249-253, 1985.
7. J. H. Siewerdsen, Signal, Noise and Detective Quantum Efficiency of a-Si:H Flat-Panel Imagers. Ann Arbor, MI: Univ, Michigan, pp. 74-88, 1998.
8. "The X-Ray Pulse Generator RIG-450 Tech, Descrption," CoRAD, St. Petersburg, Russia, 2002.
9. C. Greskovich and S. Duclos, Ceramic Scintillators. Cleveland, OH: GE Res. Development Ctr., 1996.
10. Jerald G. Graeme, "Amplifier Applications of Op Amps", McGraw Hill, 1999.
11. H. J Patrocino, J. P. Bissonnette, M. R. Bussiere and J. Schhreiner, Phys, Med, Biol, 41, pp. 239-253, 1996.
12. Wakerly, J. F., "Digital Design Principles and practices, Prentice-Hall, Englewood Cliffs, N. J, 1990.